# The cyclic dinucleotide 2′3′-cGAMP induces a broad antibacterial and antiviral response in the sea anemone *Nematostella vectensis*

Shally R. Margolis[a], Peter A. Dietzen[a], Beth M. Hayes[b], Stephen C. Wilson[a,1], Brenna C. Remick[a], Seemay Chou[b,c], and Russell E. Vance[a,d,e,f,2]

[a]Division of Immunology and Pathogenesis, Department of Molecular and Cell Biology, University of California, Berkeley, CA 94720; [b]Department of Biochemistry and Biophysics, University of California, San Francisco, CA 94158; [c]Chan Zuckerberg Biohub, San Francisco, CA 94158; [d]HHMI, University of California, Berkeley, CA 94720; [e]Immunotherapeutics and Vaccine Research Initiative, University of California, Berkeley, CA 94720; and [f]Cancer Research Laboratory, University of California, Berkeley, CA 94720

Edited by Shizuo Akira, Immunology Frontier Research Center, Osaka, Japan; received May 18, 2021; accepted November 5, 2021

**In mammals, cyclic dinucleotides (CDNs) bind and activate STING to initiate an antiviral type I interferon response. CDNs and STING originated in bacteria and are present in most animals. By contrast, interferons are believed to have emerged in vertebrates; thus, the function of CDN signaling in invertebrates is unclear. Here, we use a CDN, 2′3′ cyclic guanosine monophosphate-adenosine monophosphate (2′3′-cGAMP), to activate immune responses in a model cnidarian invertebrate, the starlet sea anemone *Nematostella vectensis*. Using RNA sequencing, we found that 2′3′-cGAMP induces robust transcription of both antiviral and antibacterial genes in *N. vectensis*. Many of the antiviral genes induced by 2′3′-cGAMP are homologs of vertebrate interferon-stimulated genes, implying that the interferon response predates the evolution of interferons. Knockdown experiments identified a role for NF-κB in specifically inducing antibacterial genes downstream of 2′3′-cGAMP. Some of these putative antibacterial genes were also found to be induced during *Pseudomonas aeruginosa* infection. We characterized the protein product of one of the putative antibacterial genes, the *N. vectensis* homolog of Dae4, and found that it has conserved antibacterial activity. This work suggests that a broad antibacterial and antiviral transcriptional response is an evolutionarily ancestral output of 2′3′-cGAMP signaling in animals.**

innate immunity | *Nematostella vectensis* | cyclic dinucleotide | NF-κB | STING

The innate immune system is an evolutionarily ancient system that detects pathogens and initiates their elimination. In mammals, the cGAS-STING pathway is critical for sensing and responding to intracellular DNA, which is particularly important for innate responses to DNA viruses (1, 2). The sensor protein in this pathway, cyclic GMP-AMP synthase (cGAS), is an enzyme that binds directly to cytosolic DNA and produces 2′3′ cyclic guanosine monophosphate-adenosine monophosphate (2′3′-cGAMP), a cyclic dinucleotide (CDN) second messenger that binds and activates STING (3–8). Active STING uses its carboxyl-terminal tail (CTT) to recruit TBK1, which then phosphorylates and activates the transcription factor IRF3 to induce the expression of type I interferons (IFNs) (9–12). Type I IFNs are secreted cytokines that signal via JAK-STAT signaling to induce transcription of hundreds of antiviral genes known as interferon-stimulated genes (ISGs) (13, 14). STING also activates NF-κB, MAP kinase (15), STAT6 (16), and autophagy-like pathways (17–20), as well as senescence (21) and cell death (22–26), although the mechanism of activation of these pathways and their importance during infection are less well understood.

Type I IFNs are thought to be a relatively recent evolutionary innovation, with identifiable interferon genes found only in vertebrates (27). In contrast, STING and cGAS are conserved in the genomes of most animals and some unicellular choanoflagellates. Remarkably, CDN to STING signaling seems to have originated in bacteria, in which it may be important in bacteriophage defense (28, 29). Studies on the function of STING in animals that lack type I IFN have been mostly limited to insects, in which STING seems to be protective during viral (30–33), bacterial (34), and microsporidial (35) infection. In insects, STING may promote defense through activation of autophagy (32, 35) and/or induction of NF-κB–dependent defense genes (30, 31, 34). Most ISGs are lacking from insect genomes and are not induced by CDN-STING signaling (31). In addition, the biochemical mechanisms of STING activation and signaling in insects remain poorly understood.

Biochemically, perhaps the best-characterized invertebrate STING protein is that of the starlet sea anemone, *Nematostella vectensis*, a member of one of the oldest animal phyla (Cnidaria). *N. vectensis* encodes a surprisingly complex genome that harbors many gene families found in vertebrates but absent in other invertebrates such as *Drosophila* (36). *N. vectensis* STING (nvSTING) and human STING adopt remarkably similar conformations when bound to 2′3′-cGAMP, and nvSTING binds to this ligand with high affinity ($K_d$ < 1nM) (37). The *N. vectensis* genome also

## Significance

Cyclic dinucleotides are signaling molecules that originated in bacteria and were subsequently acquired and co-opted by animals for immune signaling. The major cyclic dinucleotide signaling pathway in mammals results in the production of antiviral molecules called interferons. Invertebrates such as sea anemones lack interferons, and thus it was unclear whether cyclic dinucleotide signaling would play a role in immunity in these animals. Here, we report that in the anemone *Nematostella vectensis*, cyclic dinucleotides activate both antiviral and antibacterial immune responses and do so through a conserved pathway. These results provide insights into the evolutionary origins of innate immunity and suggest a broader ancestral role for cyclic dinucleotide signaling that evolved toward more specialized antiviral functions in mammals.

Author contributions: S.R.M., P.A.D., B.M.H., S.C.W., S.C., and R.E.V. designed research; S.R.M., P.A.D., B.M.H., S.C.W., and B.C.R. performed research; S.R.M., P.A.D., and B.M.H. analyzed data; and S.R.M. and R.E.V. wrote the paper.

Competing interest statement: R.E.V. consults for Ventus Therapeutics and Tempest Therapeutics.

This article is a PNAS Direct Submission.



[1]Present address: Department of Inflammation, CV & Fibrosis, Bristol Myers Squibb, Cambridge, MA 02140.

[2]To whom correspondence may be addressed. Email: rvance@berkeley.edu.

This article contains supporting information online at http://www.pnas.org/lookup/suppl/doi:10.1073/pnas.2109022118/-/DCSupplemental.

Published December 13, 2021.

encodes a cGAS enzyme that produces 2′3′-cGAMP in mammalian cell culture (17). In vertebrates, STING requires its extended CTT to initiate transcriptional responses (38, 39); however, nvSTING lacks an extended CTT, and thus its signaling mechanism and potential for inducing transcriptional responses are unclear. Based on experiments with nvSTING in mammalian cell lines, CTT-independent induction of autophagy has been proposed as the "ancestral" function of STING (17), but the endogenous function of STING in *N. vectensis* has never been described.

Despite the genomic identification of many predicted innate immune genes (40, 41), few have been functionally characterized in *N. vectensis*. The sole *N. vectensis* Toll-like receptor (TLR) is reported to bind flagellin and activate NF-κB in human cell lines and is expressed in cnidocytes, the stinging cells that define Cnidarians (42). *N. vectensis* NF-κB (nvNF-κB) binds to conserved κB sites, is inhibited by *N. vectensis* IκB (43), and seems to be required for the development of cnidocytes (44). However, no activators of endogenous nvNF-κB have yet been identified. Recent work probing the putative antiviral immune response in *N. vectensis* found that double-stranded RNA (dsRNA) injection into *N. vectensis* embryos leads to transcriptional induction of genes involved in the RNA interference (RNAi) pathway as well as genes with homology to ISGs (45). This response is partially dependent on a RIG-I–like receptor, indicating deep conservation of antiviral immunity (45). However, no antiviral or antibacterial effectors from *N. vectensis* have been functionally tested.

Here, we characterize the response of *N. vectensis* to 2′3′-cGAMP stimulation. Similar to the response of vertebrates to 2′3′-cGAMP, we find robust transcriptional induction of putative antiviral genes with homology to vertebrate ISGs. In addition, we observed induction of numerous antibacterial genes that are not induced during the vertebrate response to 2′3′-cGAMP. Although we were unable to show that the response to 2′3′-cGAMP is nvSTING dependent, we did find a selective requirement for nvNF-κB in the induction of some of the antibacterial genes. Many of these genes are also induced during *Pseudomonas aeruginosa* infection, suggesting a functional role in antibacterial immunity. We selected and characterized the antibacterial activity of one 2′3′-cGAMP–induced *Nematostella* gene product, domesticated amidase effector 4 (nvDae4), a peptidoglycan (PG)-cleaving enzyme that we found can kill gram-positive bacteria. This work demonstrates an evolutionarily ancient role for 2′3′-cGAMP in the transcriptional induction of both antiviral and antibacterial immunity.

## Results

**Transcriptional Response to 2′3′-cGAMP in *N. vectensis*.** To assess the in vivo role of 2′3′-cGAMP signaling in *N. vectensis*, we treated 2-wk-old polyps with 2′3′-cGAMP for 24 h and performed RNA sequencing (RNA-Seq) (Fig. 1*A* and *SI Appendix*, Fig. S1). Thousands of genes were induced by 2′3′-cGAMP, many of which are homologs of genes known to function in mammalian immunity. Despite the lack of associated gene ontology (GO) terms for many of the differentially regulated genes, unbiased GO term analysis revealed significant enrichment of immune-related terms (Fig. 1*B*). We also treated animals with 3′3′-linked CDNs, which are thought to be produced exclusively by bacteria and which also bind to nvSTING in vitro, albeit at lower affinity (37). Both 3′3′-cGAMP and cyclic-di-AMP treatment also induced a smaller number of genes, although all of these genes were induced more strongly by 2′3′-cGAMP (*SI Appendix*, Fig. S1). Interestingly, cyclic diguanylate monophosphate (c-di-GMP) treatment led to almost no transcriptional induction despite having relatively high affinity for nvSTING in vitro. This discrepancy may be due to differences in cell permeability among different CDNs, as the ligands were added extracellularly. In order to be able to perform subsequent genetic experiments, we confirmed that the immune gene induction downstream of 2′3′-cGAMP also occurred in embryos (which are amenable to microinjection of short hairpin RNAs [shRNAs]). qRT-PCR on 48-h embryos treated for 4 h with a lower dose of 2′3′-cGAMP revealed that many immune genes were also induced at this early developmental stage after a much shorter treatment (Fig. 1*C*).

Several interesting classes of genes were found to be up-regulated in response to 2′3′-cGAMP. For example, several genes involved in the RNAi pathway were induced, including homologs of Argonaute (AGO2), Dicer, and RNA-dependent RNA polymerase (Rdrp1). In addition, many genes that are considered ISGs in mammals were also induced in *N. vectensis*, including Viperin, RNase L, 2′-5′-oligoadenylate synthase (OAS), interferon regulatory factors (IRFs), guanylate-binding proteins (GBPs), and the putative pattern recognition receptors RIG-I–like receptor a (RLRa) and RLRb. These results suggest a conserved role for 2′3′-cGAMP signaling in antiviral immunity and ISG induction despite an apparent lack of conservation of type I IFNs in *N. vectensis*. Interestingly, we also found that many putative antibacterial genes were up-regulated in response to 2′3′-cGAMP, including homologs of LPS-binding protein (LBP), lysozyme, perforin-2, Dae4, and mucins. These results indicate that 2′3′-cGAMP stimulation leads to a broad immune response in *N. vectensis*.

To determine whether 2′3′-cGAMP signaled via nvSTING to induce these genes, we injected shRNAs targeting nvSTING into one-cell embryos and treated with 2′3′-cGAMP 48 h later. We extracted RNA and performed RNA-Seq on these samples, and surprisingly, while nvSTING transcripts were reduced by ∼50%, there was no significant impact on 2′3′-cGAMP–induced gene expression (*SI Appendix*, Fig. S2 *A* and *B*). These negative results were recapitulated in numerous independent qRT-PCR and Nanostring experiments using nine different shRNAs (three shown in *SI Appendix*, Fig. S2*C*). There are several possible explanations for the failure to observe a requirement for nvSTING in 2′3′-cGAMP signaling: 1) a twofold reduction in nvSTING transcript levels may not result in a reduction in STING protein levels if the protein is very stable; 2) even if nvSTING protein levels are reduced twofold, the reduction may not affect nvSTING signaling due to threshold effects; or 3) nvSTING may not be required for signaling downstream of 2′3′-cGAMP due the presence of a redundant 2′3′-cGAMP sensor in *N. vectensis*. We generated an anti-nvSTING antibody to validate knockdown efficiency at the protein level, but this reagent did not appear to specifically detect nvSTING in anemone lysates. We also tested whether an nvSTING translation-blocking morpholino could inhibit induction of genes in response to 2′3′-cGAMP, but this also had no effect (*SI Appendix*, Fig. S2*D*). Lastly, we made multiple attempts to generate nvSTING mutant animals using CRISPR, using multiple different guide RNAs, but the inefficiency of CRISPR in this organism and issues with mosaicism prevented the generation of nvSTING null animals. We previously solved the crystal structure of nvSTING bound to 2′3′-cGAMP and showed that binding occurs with high affinity ($K_d$ < 1nM) and in a similar mode as compared to vertebrate STING (37). In addition, we found that when expressed in mammalian cells, nvSTING forms puncta only in the presence of 2′3′-cGAMP, indicating some functional change induced by this ligand (*SI Appendix*, Fig. S2*E*). Thus, we hypothesize that 2′3′-cGAMP signals via nvSTING, but technical issues and possible redundancy with additional sensors prevent formal experimental evidence for this hypothesis.

**The *N. vectensis* NF-κB Homolog Plays a Role in the 2′3′-cGAMP Response.** We next tested the role of conserved transcription factors that are known to function downstream of STING in

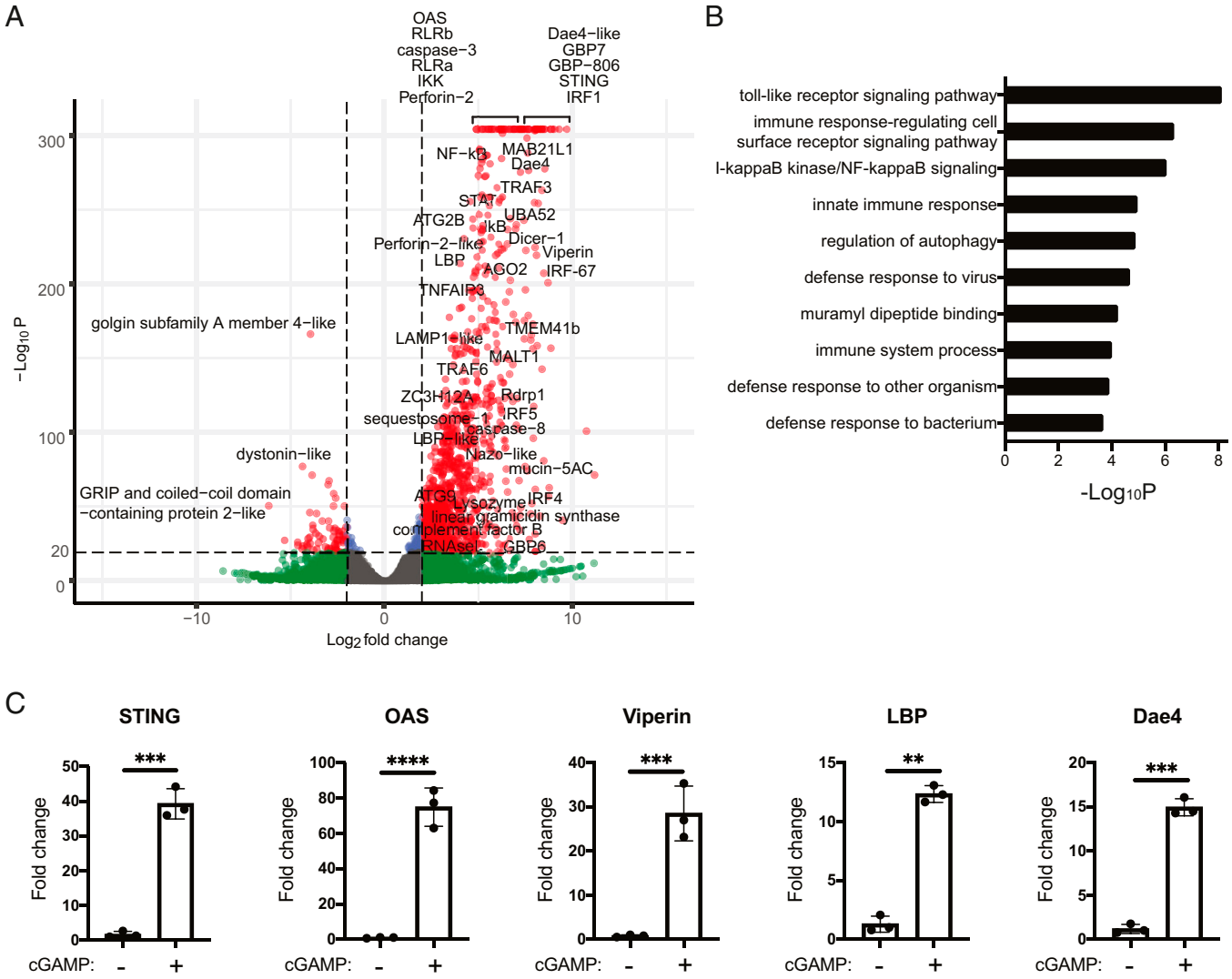


**Fig. 1.** 2′3′-cGAMP induces many putative immune genes in *N. vectensis*. (*A*) Volcano plot showing differential gene expression (DE) in *N. vectensis* polyps untreated versus treated with 2′3′-cGAMP for 24 h. A positive fold change indicates higher expression in polyps treated with 2′3′-cGAMP. Genes of interest with homologs known to be involved in immunity in other organisms are labeled. (*B*) Breakdown of DE genes into categories based on known GO terms. Gene set enrichment analysis shows a clear enrichment of GO terms associated with immunity. (*C*) qRT-PCR measuring genes of interest in 48-h-old *N. vectensis* embryos untreated or treated with 2′3′-cGAMP for 4 h. Fold changes were calculated relative to untreated as $2^{-\Delta\Delta Ct}$ and each point represents one biological replicate. Unpaired *t* test performed on ΔΔCt before log transformation. $^{**}P \leq 0.01$; $^{***}P \leq 0.001$; $^{****}P \leq 0.0001$.

mammals in the *N. vectensis* response to 2′3′-cGAMP. Interestingly, many of these transcription factors are themselves transcriptionally induced by 2′3′-cGAMP in *N. vectensis* (Fig. 1*A*). In mammals, the transcription factors IRF3 and IRF7 induce type I IFN downstream of STING activation. While the specific functions of these IRFs in interferon induction are thought to have arisen in vertebrates, other IRF family members, with conserved DNA-binding residues, are present in *N. vectensis* (*SI Appendix*, Fig. S3). We microinjected one-cell embryos with shRNAs targeting each of the five nvIRFs or a GFP control, treated with 2′3′-cGAMP, and assessed gene expression by qRT-PCR and/or Nanostring. Knockdown of IRF transcripts by 40 to 60% did not measurably impact gene induction by 2′3′-cGAMP (*SI Appendix*, Fig. S4 *A* and *B*). We similarly tested the role of the single *N. vectensis* STAT gene, as mammalian STATs both induce antiviral genes downstream of Type I IFN signaling and may even be directly activated by STING (16). Similar to the nvIRFs, we did not observe a significant loss of gene induction by 2′3′-cGAMP in nvSTAT knockdown embryos by both RNA-Seq and Nanostring (*SI Appendix*, Fig. S4 *C* and *D*). There are several explanations for these findings: 1) sufficient IRF or STAT protein may remain in knockdown animals to transduce the signal, either due to low efficiency of the knockdowns or to protein stability; 2) the IRFs may act redundantly with each other, and therefore no effect will be seen in single knockdown experiments; or 3) nvIRFs and nvSTAT may not play a role in the response to 2′3′-cGAMP.

NF-κB is also known to act downstream of mammalian STING and appears to be functionally conserved in *N. vectensis* (43). We found that NF-κB signaling components are transcriptionally induced by 2′3′-cGAMP (Fig. 1*A*). To test the role of nvNF-κB in the 2′3′-cGAMP response, we microinjected embryos with shRNAs targeting nvNF-κB, treated with 2′3′-cGAMP, and performed RNA-Seq (Fig. 2*A*). A total of 241 genes were transcribed at significantly lower levels in the nvNF-κB knockdown embryos, and of these, 98 were genes induced by 2′3′-cGAMP. Of these genes, 40 are uncharacterized, and no GO terms were significantly enriched. Of the induced genes

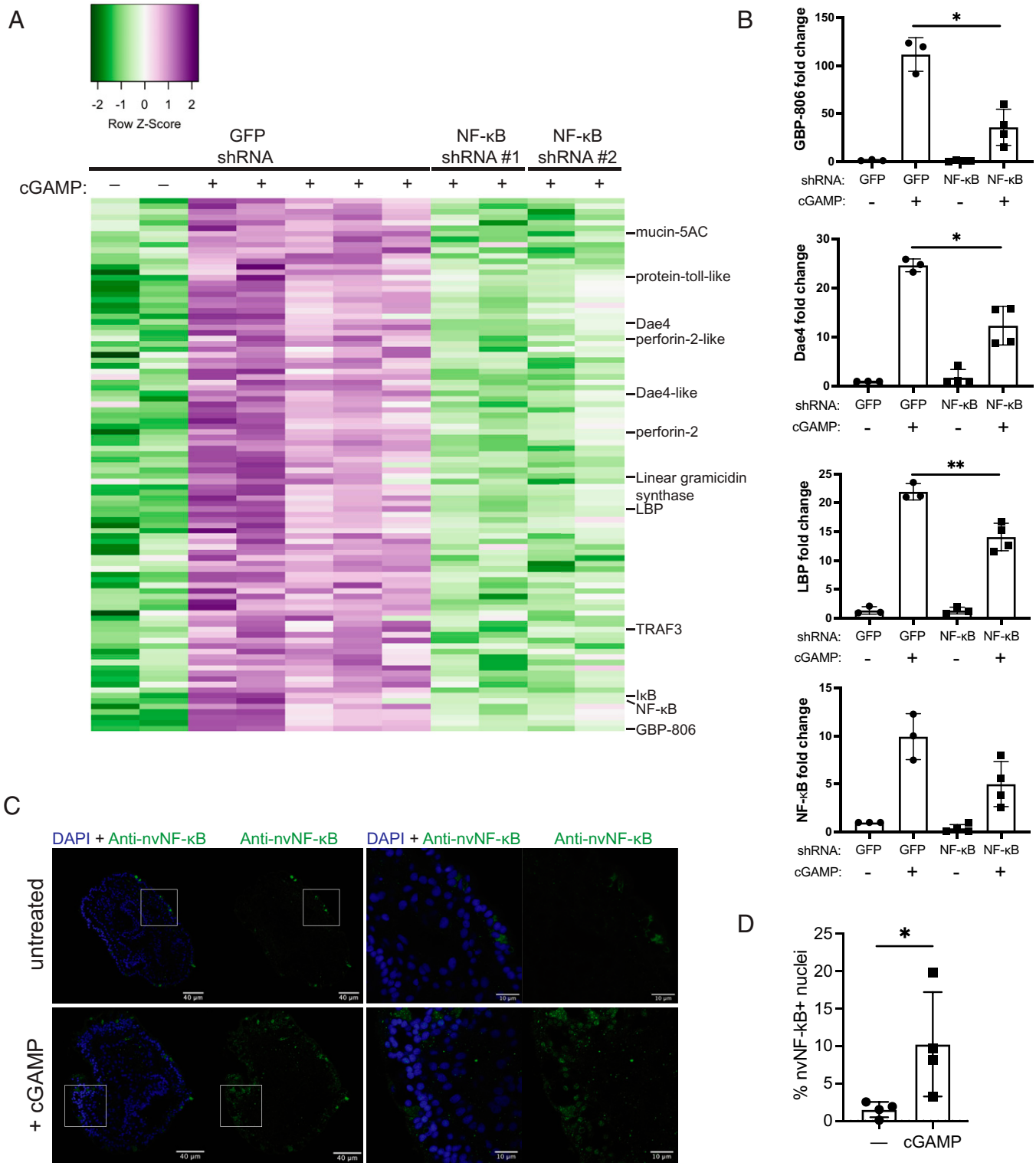


**Fig. 2.** The induction of many antibacterial genes by 2′3′-cGAMP is nvNF-κB dependent. (*A*) Heatmap showing all genes that are significantly (adjusted p value [padj] < 0.05; $\log_2$ fold change [FC] < −1) down-regulated in 2′3′-cGAMP–treated embryos microinjected with nvNF-κB shRNA versus GFP shRNA.Genes with predicted antibacterial function are labeled. (*B*) qRT-PCR of antibacterial genes in nvNF-kB shRNA– or control GFP shRNA–treated samples after induction by 2′3′-cGAMP. Fold change was calculated relative to untreated, GFP shRNA injected as $2^{-\Delta\Delta Ct}$ and each point represents one biological replicate. Unpaired *t* test performed on ΔΔCt before log transformation. $*P \leq 0.05$; $**P \leq 0.01$. (*C*) Whole mount immunofluorescence of polyps stained with anti–nvNF-κB antiserum. Right two panels are enlargements of the boxed regions indicated in the left two panels. (*D*) Quantification of cells with nuclear localization of nvNF-kB after treatment with cGAMP (representative images shown in *C*). Each point represents a single polyp, in which at least 1,500 cells were analyzed. Statistical analysis was performed by unpaired *t* test; $*P = 0.0481$.

that were annotated in the National Center for Biotechnology Information (NCBI), we noticed many were homologs of antibacterial proteins, including homologs of perforin-2/Mpeg-1, LBP, linear gramicidin synthase, and mucins. We confirmed that 2′3′-cGAMP–mediated induction of these putative antibacterial genes was nvNF-κB dependent by performing qRT-PCR (Fig. 2*B*). Notably, the induction of nvLysozyme was not nvNF-κB dependent (both by RNA-Seq and qRT-PCR; *SI Appendix*, Fig. S5*B*), indicating either the existence of another pathway for antibacterial gene induction or that our knockdown experiment was not able to affect expression of all nvNF-κB–dependent genes. In addition, all of the putative antiviral genes we examined appeared to be induced independently of nvNF-κB (*SI Appendix*, Fig. S5*A*).

We performed basic local alignment search tool (BLAST) searches of unannotated 2′3′-cGAMP–induced, nvNF-κB–dependent genes and identified several other genes with predicted antibacterial activity, including two homologs of bacterial *tae4* genes and a putative GBP (*N. vectensis* LOC5515806, hereafter nvGBP-806). The Tae4 homologs had been previously identified and will be referred to as nvDae4 proteins [discussed further in *nvDae4 Is a PG-Cleaving Enzyme with Antibacterial Activity* (46)]. To confirm the identity of nvGBP-806 as a true GBP homolog, we performed phylogenetic analysis. We identified four conserved *N. vectensis* proteins harboring an N-terminal GBP GTPase domain with conserved GBP-specific motifs, including nvGBP-806 (*SI Appendix*, Fig. S6). All of the nvGBP homologs cluster with vertebrate IFN-inducible GBPs and are themselves induced by 2′3′-cGAMP. Finally, we identified several unannotated nvNF-κB–dependent, 2′3′-cGAMP–induced genes that appeared to be cnidarian specific with no identifiable homologs in other animal phyla (*SI Appendix*, Table S1).

To test directly whether nvNF-κB is activated in *N. vectensis* upon 2′3′-cGAMP treatment, we treated polyps with cGAMP and performed immunostaining for nvNF-κB (Fig. 2*C*). Inactive NF-κB is localized to the cytosol, and we observed sparse, cytosolic staining of ectodermal cells in untreated animals, as has been previously reported (43). In contrast, in 2′3′-cGAMP–treated animals, we found many more nvNF-κB–positive cells, and in almost all of these, nvNF-κB was found in the nucleus. We performed automated quantification of nuclear nvNF-κB staining and found that ∼3 to 20% of nuclei captured in our images were positive for nvNF-κB (Fig. 2*D*). In sum, 2′3′-cGAMP leads to nvNF-κB nuclear localization, and nvNF-κB appears to be required for expression of many putative antibacterial, but not antiviral, genes. Our results demonstrate that 2′3′-cGAMP is a potent NF-κB agonist in *N. vectensis* and indicate a conserved immune function for NF-κB in this organism.

**Gene Induction During *P. aeruginosa* Challenge.** In order to test whether the putative antibacterial, NF-κB–dependent genes are induced during bacterial infection, we infected *N. vectensis* with *P. aeruginosa*, a pathogenic gram-negative bacterium. *P. aeruginosa* can infect a range of hosts, including plants, mammals, and hydra (47, 48), though infections of *N. vectensis* have not previously been reported. Infection of *N. vectensis* polyps with the *P. aeruginosa* strain PA14 led to polyp death in a dose- and temperature-dependent manner (Fig. 3*A*). A total of 48 h after infection, we isolated RNA from infected polyps and assayed gene expression. Interestingly, nvSTING expression was induced during PA14 infection (Fig. 3*B*), and many of the putative antibacterial genes we identified as 2′3′-cGAMP-induced were also induced during infection (Fig. 3*C*), although this expression was not sufficient to protect them from death. In addition, some putative antiviral genes were also induced in some animals (*SI Appendix*, Fig. S5*C*), perhaps reflecting a broader immune response in *Nematostella*. Importantly, the PA14 genome is not known to encode any proteins that produce CDNs other than c-di-GMP. Since c-di-GMP was not sufficient to robustly activate gene expression in *N. vectensis*, we believe that it is likely that the response to PA14 is independent of bacterial CDNs, although we cannot rule out an effect from PA14-produced c-di-GMP. In addition, we have no reason to believe that PA14 is activating these genes via nv-cGAS, as we do not know the activator of this enzyme. Nevertheless, taken together, these results indicate that the putative antibacterial



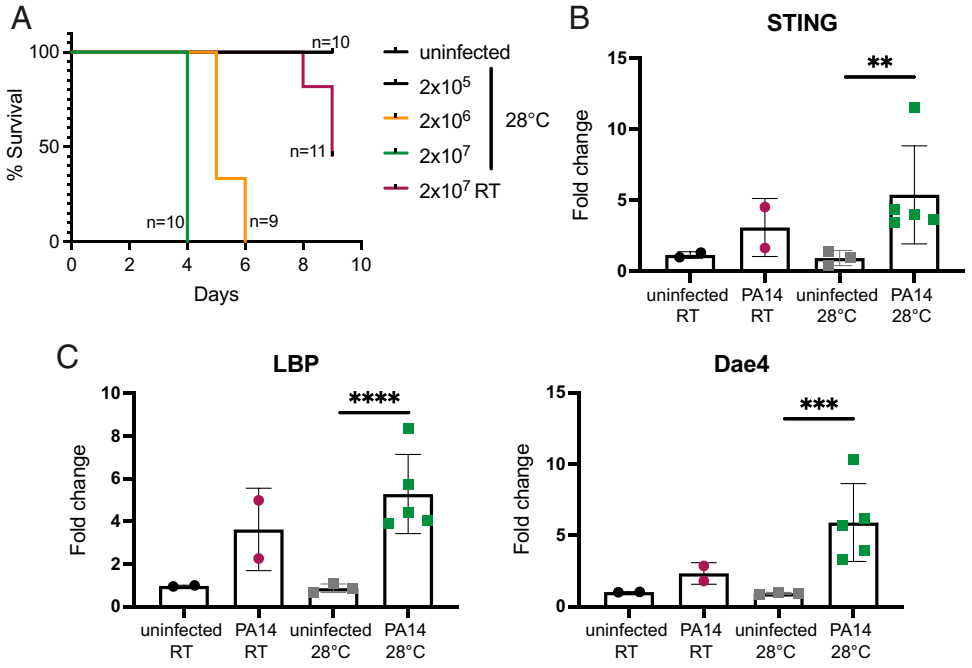


**Fig. 3.** *P. aeruginosa* infection induces putative antibacterial genes. (*A*) Survival curves of *N. vectensis* polyps infected with *P. aeruginosa* at indicated dose and temperature. (*B* and *C*) qRT-PCR of nvSTING (*B*) or putative antibacterial genes (*C*) assayed at 48 h post *P. aeruginosa* infection ($2 \times 10^7$ CFU/mL). Each point represents one biological replicate; unpaired *t* test performed on ΔΔCt before log transformation. $^{**}P \leq 0.01$; $^{***}P \leq 0.001$; $^{****}P \leq 0.0001$.

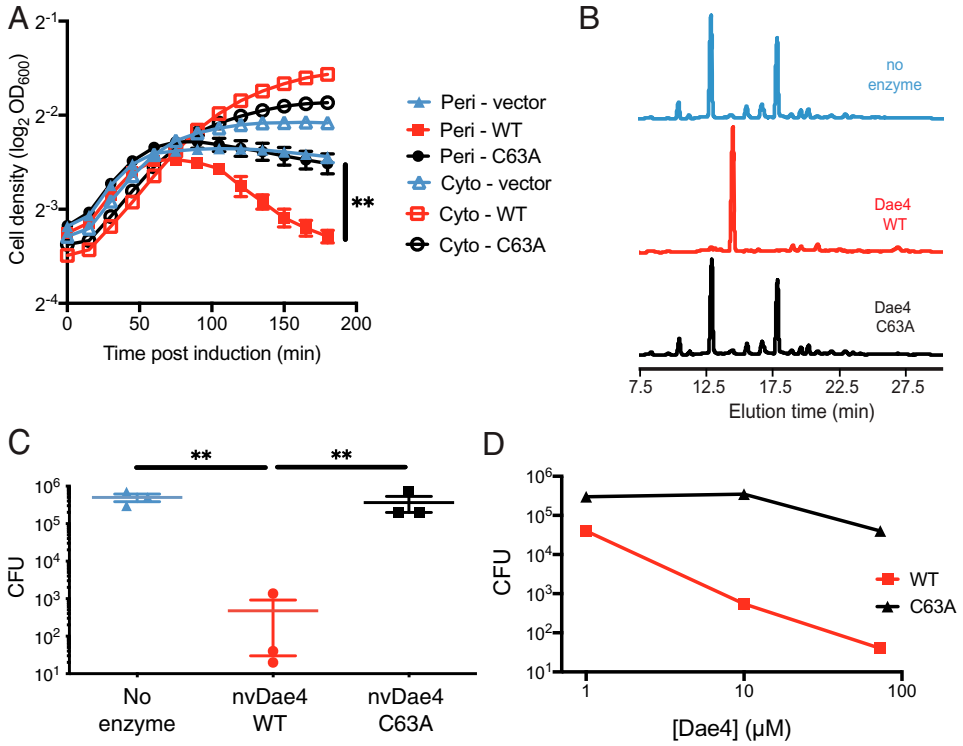


**Fig. 4.** A 2′3′-cGAMP–induced, nvNF-κB–dependent protein has antibacterial activity. (*A*) Growth of *E. coli* expressing either periplasmic (Peri-) or cytosolic (Cyto-) nvDae4 (WT or C63A) induced with 250 μM IPTG. Error bars ± SD; $n = 3$. Unpaired *t* test; $^{**}P = 0.0063$. (*B*) Partial HPLC chromatograms of *E. coli* PG sacculi after overnight incubation with buffer only (no enzyme) or 1 μM nvDae4 WT or C63A enzyme. (*C*) *B. subtilis* CFU after 2 h incubation with buffer alone, nvDae4 WT, or catalytic mutant C63A (25 μM). Error bars ± SEM; $n = 3$. Unpaired *t* test performed on log-transformed values; $^{**}P \leq 0.01$. (*D*) Dose-dependent killing of *B. subtilis* by WT nvDae4 enzyme (same assay as in *C*). Error bars ± SD; $n = 2$ per concentration.

genes we identified as induced by 2′3′-cGAMP are also induced after bacterial challenge.

**nvDae4 Is a PG-Cleaving Enzyme with Antibacterial Activity.** We decided to investigate directly whether any of the genes induced by both 2′3′-cGAMP and bacterial infection are, in fact, antibacterial. Type VI secretion amidase effector (Tae) proteins are bacterial enzymes that are injected into neighboring cells to cleave PG, an essential component of bacterial cell walls, leading to rapid cell death (49). While the *tae* genes originated in bacteria, they have been horizontally acquired multiple times in evolution by eukaryotes, and at least one of these so-called "domesticated amidase effectors" (Daes) also has bactericidal activity (46, 50). The *N. vectensis* genome has two *tae4* homologs, both of which were up-regulated by 2′3′-cGAMP in an nvNF-κB–dependent manner. However, only one of these homologs is predicted to encode a conserved catalytic cysteine (46) required for PG hydrolysis. Therefore, we focused our efforts on this homolog, which we call nvDae4 (GI: 5507694). We first tested whether nvDae4 has conserved bactericidal properties by expressing nvDae4 in *Escherichia coli* either with or without a periplasm-targeting signal sequence and measuring bacterial growth (assessed by optical density at 600nm [$OD_{600}$]) over time (Fig. 4*A*). *E. coli* are gram-negative bacteria and thus have PG compartmentalized within the periplasmic space. Consistent with the predicted PG-cleaving function of nvDae4, only periplasmic wild-type (WT), but not catalytic mutant (C63A), nvDae4 expression led to bacterial lysis. In order to test directly whether nvDae4 cleaves PG, we produced recombinant protein in insect cells. Since nvDae4 encodes a secretion signal, recombinant nvDae4 was secreted by the insect cells and purified from the cell supernatant. Purified nvDae4 protein was incubated with purified PG from either a gram-negative bacterium, *E. coli,* or a gram-positive bacterium, *Staphylococcus epidermidis*. Analysis by high-performance liquid chromatography (HPLC) showed that nvDae4 cleaves both gram-negative (Fig. 4*B*) and gram-positive (*SI Appendix*, Fig. S7) derived peptidoglycan. Finally, we wondered whether nvDae4 could directly kill gram-positive bacteria, as these bacteria contain a PG cell wall that is not protected by an outer membrane and is therefore accessible to extracellular factors. We treated *Bacillus subtilis* with recombinant nvDae4 and found that bacteria treated with WT, but not C63A nvDae4 protein, were killed (Fig. 4*C*) in a dose-dependent manner (Fig. 4*D*). Overall, these results show that the 2′3′-cGAMP–induced protein nvDae4 is a PG-cleaving enzyme with the capacity to kill bacteria.

## Discussion

In this study, we identified hundreds of *N. vectensis* genes that are induced by the STING ligand 2′3′-cGAMP. Despite over 600 million years of divergence and the absence of interferons, *N. vectensis* responds to 2′3′-cGAMP similarly to mammals by inducing a variety of antiviral genes. Similarly, Lewandowska et al. (45) recently reported that *N. vectensis* responds to the synthetic dsRN A polyinosinic-polycytidylic acid [poly(I:C)], a viral mimic and pathogen-associated molecular pattern (PAMP). In *N. vectensis*, poly(I:C) induced both RNAi pathway components and genes traditionally thought of as vertebrate ISGs. Our combined findings indicate that the pathways linking PAMP detection to ISG expression existed prior to the vertebrate innovation of type I IFNs. Interestingly, some invertebrate species have protein-based antiviral signaling pathways that perform similar functions to type I IFNs in vertebrates. For example, mosquito cells secrete the peptide Vago upon viral infection, which signals through the JAK-STAT pathway to

activate antiviral immunity (51). Additionally, the oyster *Crassostrea gigas* is thought to have an IFN-like system, but no secreted proteins have yet been identified in this organism (52). *N. vectensis* may also encode an undiscovered IFN-like protein; at a minimum, *N. vectensis* encodes several IRF-like genes (*SI Appendix*, Fig. S3). One attractive hypothesis is that these IRFs are important for the antiviral response of *N. vectensis*; however, we were unable to see any impact of single knockdown experiments on the induction of genes by 2′3′-cGAMP, though this may be explained by redundancy or technical limitations of our knockdown approach. Nevertheless, an important conclusion of our work is that induction of a broad transcriptional program is an ancestral function of 2′3′-cGAMP signaling, similar to what has been seen in *Drosophila* (31) and choanoflagellates (53). This ancestral transcriptional response complements an additional autophagy response to 2′3′-cGAMP that was previously reported to be induced by nvSTING in mammalian cells (17) and has now also been shown to be induced by 2′3′-cGAMP and STING in choanoflagellates (53).

We found that in addition to an antiviral response, *N. vectensis* responds to 2′3′-cGAMP by inducing a variety of antibacterial genes, including lysozyme, Dae4, perforin-2-like, LBP, and GBPs. With the exception of GBPs, which have dual antiviral and antibacterial activity, these antibacterial genes are not induced by 2′3′-cGAMP in vertebrates; thus, the antibacterial response appears to be a unique feature of 2′3′-cGAMP signaling in *N. vectensis*, and it will be interesting to see whether this proves true in other invertebrates or in additional cell types or contexts in vertebrates. Indeed, a recent study found that during oral *Listeria monocytogenes* infection of mice, a STING-dependent and IFN-independent response helps clear bacteria. Several of the antibacterial genes are also induced by poly(I:C) in *Nematostella* (45), and we found that at least one putative antiviral gene was also induced during *P. aeruginosa* infection, perhaps indicating a broader antipathogen response to PAMPs in *N. vectensis*. Interestingly, we found that nvNF-κB was specifically required for the induction of many of the antibacterial genes. This suggests that nvNF-κB activation downstream of 2′3′-cGAMP signaling may have been present in the most recent common ancestor of cnidarians and mammals and confirms a role for nvNF-κB in *N. vectensis* immunity. Consistent with this speculation, *Drosophila* STING also appears to activate NF-κB (30, 31, 34).

To further establish that 2′3′-cGAMP induces proteins with antibacterial activity, we functionally characterized one 2′3′-cGAMP–induced, nvNF-κB–dependent protein, nvDae4. We found that nvDae4 is a PG-cleaving enzyme with direct bactericidal activity against gram-positive bacteria. Many of the 2′3′-cGAMP–induced nvNF-κB–dependent genes are not recognizable homologs of proteins of known function; thus, they represent good candidates for the discovery of novel antibacterial genes in *N. vectensis.*

Using shRNAs to knockdown nvSTING failed to confirm an essential role for nvSTING in the response to 2′3′-cGAMP. However, our previous biochemical and structural studies showed nvSTING binds 2′3′-cGAMP with high affinity ($K_d$ < 1nM) and in a very similar manner as vertebrate STING (37). STING is essential for the response to 2′3′-cGAMP in diverse organisms including vertebrates, choanoflagellates (53), and insects (31). In addition, nvSTING is highly induced by 2′3′-cGAMP. So, despite our negative results, we favor the idea that nvSTING is at least partially responsible for the response of *N. vectensis* to 2′3′-cGAMP. It is possible that *N. vectensis* encodes a redundant 2′3′-cGAMP sensor, but such a sensor would have had to have evolved specifically in cnidarians or been lost independently from choanoflagellates, insects, and vertebrates. It is likely that technical limitations of performing shRNA knockdowns in *N. vectensis* accounts for our inability to observe a role for nvSTING in the response to 2′3′-cGAMP, though we cannot exclude the possibility that *N. vectensis* utilizes a distinct 2′3′-cGAMP-sensing pathway.

If, indeed, 2′3′-cGAMP is signaling via nvSTING, this presents several mechanistic questions. First, in mammals, all known transcriptional responses downstream of STING, including those requiring NF-κB activation, require the CTT (38, 39), leading to the question of how invertebrate STING proteins, which lack a discrete CTT, can activate this pathway. Also, nvNF-κB knockdown did not impact the vast majority of 2′3′-cGAMP–induced genes, which may imply the existence of other signaling pathways downstream of nvSTING. How these unidentified pathways become activated is another interesting question and one that could also shed light on mammalian STING signaling. Finally, mammalian STING can also be activated by direct binding to bacterial 3′3′-linked CDNs (54), and nvSTING also binds to these ligands, albeit with lower affinity (37). We found that treatment of *N. vectensis* with these ligands also led to induction of many of the same genes, likely through the same pathway. This perhaps indicates a role for the nvSTING pathway in bacterial sensing, though our preliminary attempts to observe an impact of 2′3′-cGAMP–induced gene expression on bacterial colonization of *N. vectensis* were unsuccessful. Further development of a bacterial infection model for *N. vectensis* will be required to study the antibacterial response of this organism in vivo.

A crucial remaining question is what activates nv-cGAS to produce 2′3′-cGAMP. Double-stranded DNA did not seem to activate this protein in vitro (37), but this could be due to the absence of cofactors. This protein is also constitutively active when transfected into mammalian cells, but this could be due to overexpression. Unlike human cGAS, nv-cGAS does not have any clear DNA-binding domains, although this does not necessarily exclude DNA as a possible ligand. The *Vibrio* cGAS-like enzyme DncV is regulated by folate-like molecules (55), so there is a diverse range of possible nv-cGAS activators. Understanding the role of CDN sensing pathways in diverse organisms can shed light on the mechanisms of evolution of viral and bacterial sensing and on unique ways divergent organisms have evolved to respond to pathogens.

## Methods

***N. vectensis* Culture and Spawning.** *N. vectensis* adults were a gift from Mark Q. Martindale (University of Florida, St. Augustine, FL) and were cultured and spawned as previously described (56). Briefly, animals were kept in 1/3× seawater (12 ppt salinity) in the dark at 17 °C and fed freshly hatched *Artemia* (Carolina Biological Supply Company) weekly. Spawning was induced every 2 wk by placing animals at 23 °C under bright light for 8 h, followed by 2 h in the dark, and then finally moved to the light, where they were monitored for spawning. Egg masses were de-jellied in 4% L-cysteine (pH 7 to 7.4) in 1/3× sea water for 10 to 15 min and washed three times with 1/3× sea water. Water containing sperm was added to the washed eggs, and these were either used immediately for microinjection or allowed to develop at room temperature.

**CDN Treatment.** For the RNA-Seq experiment on polyps (Fig. 1 and *SI Appendix*, Fig. S1), ~4-wk-old polyps were treated in duplicate in a bath of 500 μM c-di-AMP, c-di-GMP, 2′3′-cGAMP, or 3′3′-cGAMP (all InvivoGen) in 1/3× sea water for 24 h. For remaining cGAMP treatment experiments, 50 to 100 48-h-old embryos were treated with 100 μM 2′3′-cGAMP (InvivoGen) in 1/3× sea water for 4 h.

**RNA-Seq.** For the initial CDN treatment experiment using polyps, total RNA was extracted using Qiagen RNeasy Mini kits according to the manufacturer's protocol. Libraries were prepared by the Functional Genomics Laboratory at the University of California (UC), Berkeley using WaferGen PrepX library prep kits with oligo dT beads for messenger RNA (mRNA) enrichment according to the manufacturer's protocol, and 50-nt single-end sequencing was carried out on the HiSeq4000 (Illumina) by the Vincent J. Coates Genomics Sequencing Laboratory. For all other RNA-Seq experiments on 48-h embryos, RNA was extracted using TRIzol (Thermo Fisher Scientific) according to the

manufacturer's protocol. Libraries were prepared by the Functional Genomics Laboratory at UC Berkeley as follows: oligo dT beads from the KAPA mRNA Capture Kit (KK8581) were used for mRNA enrichment; fragmentation, adapter ligation, and complementary DNA (cDNA) synthesis were performed using the KAPA RNA HyperPrep kit (KK8540). Libraries were pooled evenly by molarity and sequenced by the Vincent J. Coates Genomics Sequencing Laboratory on a NovaSeq6000 150PE S4 flow cell (Illumina), generating 25 M read pairs per sample. Read quality was assessed using FastQC. Reads were mapped to the *N. vectensis* transcriptome (NCBI: GCF_000209225.1) using kallisto, and differential expression was analyzed in R with DESeq2. Differential expression was deemed significant with a $\log_2$ fold change greater than 1 and an adjusted *P* value less than 0.05. GO term analysis was performed using goseq with GO annotations from https://figshare.com/articles/dataset/Nematostella_vectensis_transcriptome_and_gene_models_v2_0/807696. The EnhancedVolcano package (https://github.com/kevinblighe/EnhancedVolcano) was used to generate volcano plots. Heatmaps are based on regularized log-transformed normalized counts, and Z-scores are scaled by row. All RNA-Seq results can be found in Dataset S1. Raw sequencing reads and normalized gene counts can be found at the NCBI Gene Expression Omnibus (GEO) under accession GSE175984 (57).

**qRT-PCR.** Embryos and polyps were lysed in TRIzol (Invitrogen), and RNA was extracted according to the manufacturer's protocol. A total of 500 ng RNA was treated with RQ1 RNase-free DNase (Promega) and reverse transcribed with SuperScript III (Invitrogen). qPCR was performed using SYBR Green (Thermo Fisher Scientific) with 0.8 μM of forward and reverse primers on a QuantStudio 5 Real-Time PCR System (Applied Biosystems) with the following cycling conditions: 50 °C 2 min; 95 °C 10 min; [95 °C 15 s, 60 °C 1 min] × 40; 95 °C 15 s; 60 °C 1 min; melt curve: step 0.075 °C/s to 95 °C. Fold changes in expression levels were normalized to actin and calculated using the $2^{-\Delta\Delta Ct}$ method. Student's *t* tests were performed on ΔCt values. All primer sequences used in this study can be found in Dataset S2*A*.

**shRNA Microinjection.** shRNAs for microinjection were prepared by in vitro transcription as previously described (58). Briefly, unique 19-nt targeting motifs were identified and used to create oligonucleotides with the following sequence: T7 promoter—19-nt motif—linker—antisense 19-nt motif–TT. RNA secondary structure was visualized using mfold (www.unafold.org/mfold/applications/rna-folding-form.php) to ensure a single RNA conformation. Both sense and antisense oligonucleotides were synthesized and mixed to a final concentration of 25 μM, heated to 98 °C for 5 min, and cooled to 24 °C before use as template for in vitro transcription using the Ampliscribe T7-Flash Transcription Kit (Lucigen). Reactions were allowed to proceed overnight, followed by a 15-min treatment with DNase and subsequent purification with Direct-zol RNA MiniPrep Plus (Zymo Research). All shRNAs used in this study can be found in Dataset S2*B*.

Microinjections of one-cell embryos were carried out as previously described (59). shRNAs were diluted to a concentration of 500 to 900 ng/μL (ideal concentrations were determined experimentally) in RNase-free water with fluorescent dextran for visualization. Injected embryos were monitored for gross normal development at room temperature and used for experiments 48 h later unless otherwise indicated. Knockdowns for each gene were performed using at least two different shRNAs, and phenotypes were confirmed in at least three independent experiments.

**Immunohistochemistry, Imaging, and Quantification.** Polyps treated for 4 h with 100 μM 2′3′-cGAMP were stained for nvNF-κB as previously described (60). Briefly, polyps were fixed in 4% paraformaldehyde in 1/3× sea water overnight at 4 °C with rocking and subsequently washed three times with wash buffer (1× phosphate-buffered saline [PBS], 0.2% Triton X-100). Antigen retrieval was performed by placing anemones in 95 °C 5% urea for 5 min and allowing them to cool to room temperature before washing three times in wash buffer. Samples were blocked overnight at 4 °C in blocking buffer (1× PBS, 5% normal goat serum, 1% bovine serum albumin, 0.2% Triton X-100). Samples were stained with anti–nvNF-κB (1:100; gift of Thomas Gilmore, Boston University, Boston, MA) in blocking buffer for 90 min at room temperature and washed four times in wash buffer. Samples were then incubated in fluorescein isothiocyanate (FITC)-anti-Rabbit immunoglobulin G (IgG) (1:160; F9887, Sigma-Aldrich) in blocking buffer for 90 min at 37 °C. Finally, samples were washed in wash buffer, stained with 1 μg/mL DAPI for 10 min, washed again, and mounted in Vectashield HardSet Mounting medium and imaged on a Zeiss LSM 710 AxioObserver. Imaris 9.2 (Bitplane) was used to create three-dimensional surfaces based on DAPI expression, and surface statistics were exported and analyzed in FlowJo (BD Biosciences) to quantify nuclear nvNF-κB expression as previously described (61).

**Bacterial Infection.** Single colonies of *P. aeruginosa* strain PA14-GFP were cultured overnight in Lysogeny Broth (LB) with 50 μg/mL of carbenicillin, centrifuged for 5 min at 3,000 × *g*, resuspended to an $OD_{600}$ of 0.1, 0.01, or 0.001 in 1/3× sea water and used to infect polyps, which were kept at room temperature or 28 °C as indicated. Inputs were plated to calculate colony-forming units (CFU) per mL. Polyp survival was monitored daily. For expression analysis, polyps were homogenized in TRIzol and RNA extraction and qPCR were performed as indicated in *qRT-PCR*.

**Protein Purification.** nvDae4 lacking its signal peptide was cloned from cDNA. This fragment was then cloned into the pAcGP67-A baculovirus transfer vector for secreted, His-tagged protein expression. The plasmid for expressing mutant nvDae4 (C63A) was made from the pAcGP67-A-nvDae4 plasmid using Q5 site-directed mutagenesis (New England Biolabs) according to the manufacturer's protocol. Plasmids were transfected into Sf9 insect cells ($2 \times 10^6$ cells/mL in 2 mL) using Cellfectin II Reagent (Gibco) along with BestBac 2.0 v-cath/chiA Deleted Linearized Baculovirus DNA (Expression Systems) for 6 h, after which media were replaced and cells were left for 1 wk at 25 °C. Supernatants were harvested, and 50 μL was used to infect $7 \times 10^6$ Sf9 cells in 10 mL media for 1 wk at 25 °C. Supernatants containing secondary virus were harvested, tested, and used to infect High Five cells (2 L at $1.5 \times 10^6$ cells/mL) for 72 h at 25 °C with shaking. Supernatants containing protein were harvested by centrifuging for 15 min at 600 × *g* at 4 °C and subsequently passing through a 0.45-μm filter to remove all cells. Supernatants were buffered to 1× 4-(2-hydroxyethyl)-1-piperazineethanesulfonic acid (HEPES) buffered saline (HBS) (20 mM HEPES pH 7.2, 150 mM NaCl), mixed with 2 mL Ni-NTA agarose per liter, and rotated at 4 °C for 2 h. Ni-NTA resins with bound protein were collected on a column by gravity flow and washed with 30× column volume of wash buffer (20 mM HEPES, 1M NaCl, 30 mM imidazole, 10% glycerol). Protein was eluted in 1 mL fractions using 1× HBS supplemented with 200 mM imidazole. Buffer was exchanged to 1× HBS+ 2mM dithiothreitol (DTT) using Econo-Pac10DG Desalting Prepacked Gravity Flow Columns (Bio-Rad) according to the manufacturers protocol, and proteins were concentrated using 10-kDa concentrators (Millipore).

**Bacterial Killing Assays.** For expression in *E. coli*, nvDae4 WT and C63A lacking the endogenous signal sequence were cloned into the pET28a vector for inducible cytosolic expression or the pET22b vector for inducible periplasmic expression. *E. coli* (BL21 DE3 strain) were freshly transformed with the vectors and grown overnight in LB with 50 μg/mL kanamycin (for pET28a-transformed cultures) or carbenicillin (for pET22b-transformed cultures) shaking at 37 °C. Overnight cultures were back-diluted in LB to the same $OD_{600}$ and grown to log phase before induction with 0.25 mM isopropyl β-d-1-thiogalactopyranoside (IPTG). Plates were kept shaking at 37 °C, and $OD_{600}$ was read every 5 min for 3 h.

*B. subtilis*-GFP (derivative of strain 168; Bacillus Genetic Stock Center accession No. 1A1139) was grown to log phase in LB with 100 μg/mL spectinomycin, centrifuged, resuspended in 0.5× HBS, and incubated alone or with nvDae4 WT or C63A at indicated concentrations for 2 to 3 h at 37 °C. Serial dilutions were plated on LB agar with 100 μg/mL spectinomycin to determine CFU.

**PG Cleavage Assays.** PG was purified and analyzed as previously described (50). Briefly, *E. coli* BW11325 (from Carol Gross, UC San Francisco, CA) and *S. epidermis* BCM060 (from Tiffany Scharschmidt, UC San Francisco, CA) were grown to an $OD_{600}$ of 0.6, harvested by centrifugation, and boiled in sodium dodecyl sulphate (SDS; 4% final concentration) for 4 h with stirring. After washing in purified water to remove SDS, the PG was treated with Pronase E for 2 h at 60 °C (0.1 mg/mL final concentration in 10 mM Tris·HCl pH 7.2 and 0.06% NaCl; preactivated for 2 h at 60 °C). Pronase E was heat inactivated at 100 °C for 10 min and washed with sterile filtered water (5 × 20 min at 21,000 × *g*). PG from gram-positive bacteria (*Se*) was also treated with 48% hydrofluoric acid (HF) at 37 °C for 48 h to remove teichoic acids, followed by washes with sterile filtered water. nvDae4 enzyme (WT and C63A) was added (1 to 10 μM in 10 mM Tris·HCl pH 7.2 and 0.06% NaCl) and incubated overnight at 37 °C. Enzymes were heat inactivated at 100 °C for 10 min. Mutanolysin (Sigma M9901, final concentration 20 μg/mL) was added to the purified PG and incubated overnight at 37 °C. The PG fragments were reduced, acidified, and analyzed via HPLC (0.5 mL/min flow rate, 55 °C with Hypersil ODS C18 HPLC column, Thermo Fisher Scientific, catalog number: 30103-254630).

**Phylogenetic Analysis.** Protein sequences containing domains of interest were downloaded from NCBI, with the exception of nvGBP6 and nvGBP7, for which RNA-Seq data showed additional nucleotide usage relative to the reference sequence (all sequences can be found in Dataset S2C). These were aligned on phylogeny.fr using MUSCLE and manipulated in Geneious. For the GBP and IRF alignments, only the domain of interest was used for phylogenetic analysis. Maximum likelihood phylogenetic trees were generated with PhyML using

100 bootstrap replicates. Alignments shown were made in Geneious using Clustal Omega.

**Nanostring Gene Expression Analysis.** A custom codeset targeting 36 genes of interest and 4 housekeeping genes for normalization (Dataset S2*D*) was designed by NanoString Technologies for use in nCounter XT CodeSet Gene Expression Assays run on an nCounter SPRINT Profiler (NanoString Technologies). RNA was isolated as it was for qRT-PCR experiments and hybridized to probes according to the manufacturer's protocol using 50 ng/μL total RNA. Quality control, data normalization, and visualization were performed in nSolver 4.0 analysis software (NanoString Technologies) according to the manufacturer's protocol.

**Mammalian Cell Immunofluorescence and Confocal Microscopy.** Glass coverslips were seeded with 293T cells and grown to ∼50% confluency. Cells were transfected for 24 to 48 h with a total of 1.25 μg DNA and 3 μL Lipofectamine 2000. Each well contained the following: pcDNA4-STING (10 ng), pEGFP-LC3 (5 ng), and either empty vector or pcDNA4 with the indicated cyclic dinucleotide synthase (1,235 ng). Cells were washed once in PBS, fixed for 15 min in 4% paraformaldehyde, washed once in PBS, and permeabilized for 5 min in 0.5% saponin in PBS. Cells were then washed once in PBS and treated with 0.1% sodium borohydride/0.1% saponin/PBS for 5 to 10 min in order to consume any remaining paraformaldehyde. Cells were then washed three times in PBS and blocked with blocking buffer (1% BSA/0.1% saponin/PBS) for 45 min. Cells were then incubated with hemagglutinin (HA) antibody (1:200 dilution, Sigma 11867423001 rat IgG from Roche) in blocking buffer for 1 h and washed three times in PBS. Each well was then incubated with 0.1% saponin/PBS and secondary antibody (1:500 dilution, Jackson ImmunoResearch, Cy3 affinipure donkey anti-rat IgG, 712-165-153) for 45 min. Finally, cells were washed three times in PBS, mounted using VectaShield with DAPI, and dried overnight. Images were acquired using a Zeiss LSM 780 NLO AxioExaminer.

**Data Availability.** RNA-Seq data have been deposited in NCBI GEO (GSE175984).

**ACKNOWLEDGMENTS.** We thank Mark Q. Martindale and Miguel Salinas-Saavedra for *N. vectensis* animals and training. We also thank Matt Gibson for sharing shRNA protocols and Thomas Gilmore for the anti–nvNF-κB antibody. We thank members of the R.E.V. and Barton laboratories for discussions and Arielle Woznica for comments on the manuscript. This work used the Functional Genomic Laboratory and Vincent J. Coates Genomics Sequencing Laboratory at UC Berkeley, supported by the NIH S10 OD018174 Instrumentation Grant. Confocal imaging experiments were conducted at the Cancer Research Laboratory Molecular Imaging Center supported by the Gordon and Betty Moore Foundation; we would like to thank Holly Aaron and Feather Ives for training and assistance. R.E.V. is an HHMI Investigator and is supported by NIH Grants AI0663302, AI075039, and AI155634. S.R.M. was supported by the NSF Graduate Research Fellowship under Grant Nos. DGE 1106400 and DGE 1752814. B.M.H. and S.C. were supported by funding from the NIH (R01AI132851 to S.C.), the Chan Zuckerberg Biohub, and the Sangvhi-Agarwal Innovation Award. Any opinions, findings, and conclusions or recommendations expressed in this material are those of the authors and do not necessarily reflect the views of the NSF, HHMI, or the NIH.



1. J. Ahn, G. N. Barber, STING signaling and host defense against microbial infection. *Exp. Mol. Med.* **51**, 1–10 (2019).
2. A. Ablasser, Z. J. Chen, cGAS in action: Expanding roles in immunity and inflammation. *Science* **363**, eaat8657 (2019).
3. L. Sun, J. Wu, F. Du, X. Chen, Z. J. Chen, Cyclic GMP-AMP synthase is a cytosolic DNA sensor that activates the type I interferon pathway. *Science* **339**, 786–791 (2013).
4. P. Gao *et al.*, Cyclic [G(2′,5′)pA(3′,5′)p] is the metazoan second messenger produced by DNA-activated cyclic GMP-AMP synthase. *Cell* **153**, 1094–1107 (2013).
5. A. Ablasser *et al.*, cGAS produces a 2′-5′-linked cyclic dinucleotide second messenger that activates STING. *Nature* **498**, 380–384 (2013).
6. E. J. Diner *et al.*, The innate immune DNA sensor cGAS produces a noncanonical cyclic dinucleotide that activates human STING. *Cell Rep.* **3**, 1355–1361 (2013).
7. X. Zhang *et al.*, Cyclic GMP-AMP containing mixed phosphodiester linkages is an endogenous high-affinity ligand for STING. *Mol. Cell* **51**, 226–235 (2013).
8. H. Ishikawa, G. N. Barber, STING is an endoplasmic reticulum adaptor that facilitates innate immune signalling. *Nature* **455**, 674–678 (2008).
9. Y. Tanaka, Z. J. Chen, STING specifies IRF3 phosphorylation by TBK1 in the cytosolic DNA signaling pathway. *Sci. Signal.* **5**, ra20 (2012).
10. S. Liu *et al.*, Phosphorylation of innate immune adaptor proteins MAVS, STING, and TRIF induces IRF3 activation. *Science* **347**, aaa2630 (2015).
11. C. Zhang *et al.*, Structural basis of STING binding with and phosphorylation by TBK1. *Nature* **567**, 394–398 (2019).
12. B. Zhao *et al.*, A conserved PLPLRT/SD motif of STING mediates the recruitment and activation of TBK1. *Nature* **569**, 718–722 (2019).
13. D. B. Stetson, R. Medzhitov, Type I interferons in host defense. *Immunity* **25**, 373–381 (2006).
14. J. W. Schoggins, Interferon-stimulated genes: What do they all do? *Annu. Rev. Virol.* **6**, 567–584 (2019).
15. T. Abe, G. N. Barber, Cytosolic-DNA-mediated, STING-dependent proinflammatory gene induction necessitates canonical NF-κB activation through TBK1. *J. Virol.* **88**, 5328–5341 (2014).
16. H. Chen *et al.*, Activation of STAT6 by STING is critical for antiviral innate immunity. *Cell* **147**, 436–446 (2011).
17. X. Gui *et al.*, Autophagy induction via STING trafficking is a primordial function of the cGAS pathway. *Nature* **567**, 262–266 (2019).
18. T. D. Fischer, C. Wang, B. S. Padman, M. Lazarou, R. J. Youle, STING induces LC3B lipidation onto single-membrane vesicles via the V-ATPase and ATG16L1-WD40 domain. *J. Cell Biol.* **219**, e202009128 (2020).
19. R. O. Watson, P. S. Manzanillo, J. S. Cox, M. Extracellular, Extracellular *M. tuberculosis* DNA targets bacteria for autophagy by activating the host DNA-sensing pathway. *Cell* **150**, 803–815 (2012).
20. R. O. Watson *et al.*, The cytosolic sensor cGAS detects *Mycobacterium tuberculosis* DNA to induce type I interferons and activate autophagy. *Cell Host Microbe* **17**, 811–819 (2015).
21. S. Glück, A. Ablasser, Innate immunosensing of DNA in cellular senescence. *Curr. Opin. Immunol.* **56**, 31–36 (2019).
22. M. M. Gaidt *et al.*, The DNA inflammasome in human myeloid cells is initiated by a STING-cell death program upstream of NLRP3. *Cell* **171**, 1110–1124.e18 (2017).
23. A. Sze *et al.*, Host restriction factor SAMHD1 limits human T cell leukemia virus type 1 infection of monocytes via STING-mediated apoptosis. *Cell Host Microbe* **14**, 422–434 (2013).
24. S. R. Paludan, L. S. Reinert, V. Hornung, DNA-stimulated cell death: Implications for host defence, inflammatory diseases and cancer. *Nat. Rev. Immunol.* **19**, 141–153 (2019).
25. M. F. Gulen *et al.*, Signalling strength determines proapoptotic functions of STING. *Nat. Commun.* **8**, 427 (2017).
26. J. Wu *et al.*, STING-mediated disruption of calcium homeostasis chronically activates ER stress and primes T cell death. *J. Exp. Med.* **216**, 867–883 (2019).
27. S. R. Margolis, S. C. Wilson, R. E. Vance, Evolutionary origins of cGAS-STING signaling. *Trends Immunol.* **38**, 733–743 (2017).
28. D. Cohen *et al.*, Cyclic GMP-AMP signalling protects bacteria against viral infection. *Nature* **574**, 691–695 (2019).
29. B. R. Morehouse *et al.*, STING cyclic dinucleotide sensing originated in bacteria. *Nature* **586**, 429–433 (2020).
30. A. Goto *et al.*, The kinase IKKβ regulates a STING- and NF-κB-dependent antiviral response pathway in Drosophila. *Immunity* **49**, 225–234.e4 (2018).
31. H. Cai *et al.*, 2′3′-cGAMP triggers a STING- and NF-κB-dependent broad antiviral response in *Drosophila*. *Sci. Signal.* **13**, eabc4537 (2020).
32. Y. Liu *et al.*, Inflammation-induced, STING-dependent autophagy restricts Zika virus infection in the Drosophila brain. *Cell Host Microbe* **24**, 57–68.e3 (2018).
33. X. Hua *et al.*, Stimulator of interferon genes (STING) provides insect antiviral immunity by promoting Dredd caspase-mediated NF-κB activation. *J. Biol. Chem.* **293**, 11878–11890 (2018).
34. M. Martin, A. Hiroyasu, R. M. Guzman, S. A. Roberts, A. G. Goodman, Analysis of Drosophila STING reveals an evolutionarily conserved antimicrobial function. *Cell Rep.* **23**, 3537–3550.e6 (2018).
35. X. Hua, W. Xu, S. Ma, Q. Xia, STING-dependent autophagy suppresses *Nosema bombycis* infection in silkworms, *Bombyx mori*. *Dev. Comp. Immunol.* **115**, 103862 (2021).
36. N. H. Putnam *et al.*, Sea anemone genome reveals ancestral eumetazoan gene repertoire and genomic organization. *Science* **317**, 86–94 (2007).
37. P. J. Kranzusch *et al.*, Ancient origin of cGAS-STING reveals mechanism of universal 2′,3′ cGAMP signaling. *Mol. Cell* **59**, 891–903 (2015).
38. L. H. Yamashiro *et al.*, Interferon-independent STING signaling promotes resistance to HSV-1 in vivo. *Nat. Commun.* **11**, 3382 (2020).
39. S. Yum, M. Li, Y. Fang, Z. J. Chen, TBK1 recruitment to STING activates both IRF3 and NF-kappaB that mediate immune defense against tumors and viral infections. *Proc. Natl. Acad. Sci. U.S.A.* **118**, e2100225118 (2021).
40. D. J. Miller *et al.*, The innate immune repertoire in Cnidaria—Ancestral complexity and stochastic gene loss. *Genome Biol.* **8**, R59 (2007).
41. A. M. Reitzel, J. C. Sullivan, N. Traylor-Knowles, J. R. Finnerty, Genomic survey of candidate stress-response genes in the estuarine anemone *Nematostella vectensis*. *Biol. Bull.* **214**, 233–254 (2008).
42. J. J. Brennan *et al.*, Sea anemone model has a single Toll-like receptor that can function in pathogen detection, NF-κB signal transduction, and development. *Proc. Natl. Acad. Sci. U.S.A.* **114**, E10122–E10131 (2017).
43. F. S. Wolenski *et al.*, Characterization of the core elements of the NF-κB signaling pathway of the sea anemone *Nematostella vectensis*. *Mol. Cell. Biol.* **31**, 1076–1087 (2011).
44. F. S. Wolenski, C. A. Bradham, J. R. Finnerty, T. D. Gilmore, NF-κB is required for Cnidocyte development in the sea anemone *Nematostella vectensis*. *Dev. Biol.* **373**, 205–215 (2013).
45. M. Lewandowska, T. Sharoni, Y. Admoni, R. Aharoni, Y. Moran, Functional characterization of the cnidarian antiviral immune response reveals ancestral complexity. *Mol. Biol. Evol.* **38**, 4546–4561 (2021).

46. S. Chou *et al.*, Transferred interbacterial antagonism genes augment eukaryotic innate immune function. *Nature* **518**, 98–101 (2015).
47. L. G. Rahme *et al.*, Plants and animals share functionally common bacterial virulence factors. *Proc. Natl. Acad. Sci. U.S.A.* **97**, 8815–8821 (2000).
48. S. Franzenburg *et al.*, MyD88-deficient Hydra reveal an ancient function of TLR signaling in sensing bacterial colonizers. *Proc. Natl. Acad. Sci. U.S.A.* **109**, 19374–19379 (2012).
49. A. B. Russell *et al.*, Type VI secretion delivers bacteriolytic effectors to target cells. *Nature* **475**, 343–347 (2011).
50. B. M. Hayes *et al.*, Ticks resist skin commensals with immune factor of bacterial origin. *Cell* **183**, 1562–1571.e1512 (2020).
51. P. N. Paradkar, L. Trinidad, R. Voysey, J. B. Duchemin, P. J. Walker, Secreted Vago restricts West Nile virus infection in Culex mosquito cells by activating the Jak-STAT pathway. *Proc. Natl. Acad. Sci. U.S.A.* **109**, 18915–18920 (2012).
52. T. J. Green, P. Speck, Antiviral defense and innate immune memory in the oyster. *Viruses* **10**, 133 (2018).
53. A. Woznica *et al.*, STING mediates immune responses in the closest living relatives of animals. *eLife* **10**, e70436 (2021).
54. D. L. Burdette *et al.*, STING is a direct innate immune sensor of cyclic di-GMP. *Nature* **478**, 515–518 (2011).
55. D. Zhu *et al.*, Structural biochemistry of a *Vibrio cholerae* dinucleotide cyclase reveals cyclase activity regulation by folates. *Mol. Cell* **55**, 931–937 (2014).
56. D. J. Stefanik, L. E. Friedman, J. R. Finnerty, Collecting, rearing, spawning and inducing regeneration of the starlet sea anemone, *Nematostella vectensis*. *Nat. Protoc.* **8**, 916–923 (2013).
57. S. R. Margolis, Cyclic dinucleotide stimulation of Nematostella vectensis. Gene Expression Omnibus. https://www.ncbi.nlm.nih.gov/geo/query/acc.cgi?acc=GSE175984. Deposited 2 June 2021.
58. A. Karabulut, S. He, C. Y. Chen, S. A. McKinney, M. C. Gibson, Electroporation of short hairpin RNAs for rapid and efficient gene knockdown in the starlet sea anemone, *Nematostella vectensis*. *Dev. Biol.* **448**, 7–15 (2019).
59. M. J. Layden, E. Röttinger, F. S. Wolenski, T. D. Gilmore, M. Q. Martindale, Microinjection of mRNA or morpholinos for reverse genetic analysis in the starlet sea anemone, *Nematostella vectensis*. *Nat. Protoc.* **8**, 924–934 (2013).
60. F. S. Wolenski, M. J. Layden, M. Q. Martindale, T. D. Gilmore, J. R. Finnerty, Characterizing the spatiotemporal expression of RNAs and proteins in the starlet sea anemone, *Nematostella vectensis*. *Nat. Protoc.* **8**, 900–915 (2013).
61. D. I. Kotov, T. Pengo, J. S. Mitchell, M. J. Gastinger, M. K. Jenkins, Chrysalis: A new method for high-throughput histo-cytometry analysis of images and movies. *J. Immunol.* **202**, 300–308 (2019).